



Small-scale characterisation of irradiated nuclear materials: Part I – Microstructure



P.D. Edmondson*, A. London, A. Xu, D.E.J. Armstrong, S.G. Roberts

Department of Materials, University of Oxford, Parks Road, Oxford OX1 3PH, UK

ARTICLE INFO

Article history:

Available online 26 November 2014

ABSTRACT

The behaviour of nanometre-scale precipitates in oxide dispersion strengthened (ODS) ferritic alloys and tungsten–rhenium alloys for nuclear applications has been examined by atom probe tomography (APT). Low Re content tungsten alloys showed no evidence of Re clustering following self-ion irradiation whereas the 25 at.% Re resulted in cluster formation. The size and composition of clusters varied depending on the material form during irradiation (pre-sharpened needle or bulk). These results highlight the care that must be taken in interpreting data from ion irradiated pre-sharpened needles due to the presence of free surfaces. Self-ion irradiation of the ODS ferritic alloy resulted in a change in the composition of the clusters, indicating a transition from a near-stoichiometric $\text{Y}_2\text{Ti}_2\text{O}_7$ composition towards a Ti_2YO_5 .

Published by Elsevier B.V.

1. Introduction

The next generation of nuclear reactors – both fission and fusion – will see the materials from which they are constructed being subjected to greater extremes than those currently in service; these extremes primarily being high temperatures and greater damage levels [1,2]. As such it is necessary to develop new materials that can withstand these extremes more than the materials that are currently in use today. Two highly prominent materials for advanced reactor designs are oxide dispersion strengthened ferritic alloys (including the nanostructured ferritic alloy class) and tungsten. Both of these materials can suffer from radiation-induced microstructural changes that are detrimental to the mechanical properties of the alloys.

1.1. Tungsten

Tungsten is the prime candidate material for the plasma facing components (PFCs) of future fusion devices such as ITER and DEMO [3–5]. During operations the deuterium–tritium reaction results in the production of 14.1 MeV energetic neutrons that may interact with the PFC material. This interaction can result in two types of material modification: lattice damage caused by the permanent displacement of atoms from their lattice sites, and transmutation reactions whereby the matrix atoms are chemically altered into

another element. The lattice damage generated will take the form of fundamental defects e.g. interstitials and vacancies, and more complex defects such as dislocations, stacking faults and voids. Chemical transmutation occurs as a function of neutron energy and fluence [6]. It has been predicted that under fusion-like conditions the most common transmutation products from a pure tungsten component after 5 years of full-power operation will include W, Re, Os, Ta, Hf, He and H [4,6] with the most common transmutation products being Re and Os (5 and 3 at.% respectively after 5 years operation).

Pure tungsten is inherently brittle at low temperatures (~ 400 – 500 °C [7,8]) but through alloying with Re the brittle-to-ductile transition temperature can be reduced. Therefore the production of Re due to transmutation should be beneficial. However the displacing irradiation can result in radiation-enhanced clustering of the transmutation products [9]. The resulting clusters can be σ or χ phases (ReW and Re_3W respectively) that can facilitate embrittlement [9]. It is therefore necessary to understand the parameter space within which W–Re (and W–Re–Os) cluster formation occurs so that steps can be taken to mitigate the diminution of mechanical properties.

1.2. Oxide dispersion strengthened ferritic alloys

The class of steels known as oxide dispersion strengthened (ODS) ferritic alloys (also known as nanostructured ferritic alloys) consist of a dispersion of ultra-fine oxide particles throughout the matrix. These oxide particles serve to improve the mechanical properties of the system, particularly at high temperatures, of the

* Corresponding author at: Materials Science and Technology Division, Oak Ridge National Laboratory, Oak Ridge, TN 37831, USA.

E-mail address: edmondsonpd@ornl.gov (P.D. Edmondson).

system through inhibiting dislocation motion and grain boundary sliding. In nuclear applications the oxide particles have been suggested to act as point defect sinks [10,11] to improve radiation tolerance, and as preferential sites for the formation of nano-scale He bubbles therefore reducing swelling compared to non-ODS steels [12–15]. The ability of the oxide particles to improve these properties depends on the structure and composition of the particles [10,11,16,17] and their stability under irradiation. Typical compositions of ODS steels include between 9 and 14 at.% Cr for oxidation resistance (most commonly 14 at.%); W for solid solution hardening; Y_2O_3 that is put into solid solution during the initial, mechanical alloying, process but then during consolidation at high temperatures forms precipitates; and Ti to inhibit significant growth of the oxide particles; the balance being made up of Fe and impurities [18]. For this reason these steels are often referred to as 14YWT, reflecting the constituent elements.

Previous studies of the radiation behaviour of the particles under irradiation [19,20] showed that at temperatures of 100 °C and below, oxide particles can be dissolved back into the matrix whereas at higher temperatures, refinement and growth can be observed [21,22]. This clearly indicates that the radiation has some effect on the oxide particles, and that a more detailed understanding of this radiation response is required.

2. Experimental methods

2.1. Tungsten

The tungsten materials used in this study came in the form of wire or bulk specimens. The alloy wires were 0.25 mm in diameter with compositions of W–3 wt.%Re, W–5 wt.%Re and W–25 wt.%Re (W–3Re, W–5Re, and W–25Re respectively); purchased from Goodfellow and with a total impurity concentration below ~210 ppm. The wires were annealed at 1400 °C for 12 h to ensure a dislocation free structure prior to electropolishing in a 5 wt.% NaOH solution to form a needle for atom probe analysis.

Bulk samples of W–25Re were prepared by vacuum arc melting of tungsten (Sigma Aldrich) and rhenium (AEE) powders. The impurity levels of the material was determined by X-ray fluorescence to be below ~210 ppm [23]. The surface of the bulk material was mechanically polished to a mirror-like finish using colloidal silica as the final polishing medium.

Both bulk and needle-shaped specimens were irradiated with 2 MeV W ions to a fluence of 1×10^{14} ions cm^{-2} (equivalent to 1.5 displacements per atom, dpa) at temperatures of 300 and 500 °C using the Tandem accelerator at the University of Surrey Ion Beam Centre. During irradiation the needle-shaped specimens were orientated parallel to the direction of the ion beam i.e. the irradiation was head-on to the apex of the needle. The ion fluences were converted to damage levels in dpa using information obtained using the Stopping and Ranges of Ions in Matter (SRIM) simulation program [24] using the Kinchin–Pease model and a displacement energy, E_d , of 68 eV [25].

Following ion irradiation the samples were prepared from the bulk material for atom probe analysis using a focussed ion beam (FIB) technique [26]. Samples from both bulk and needle-shaped specimens were analysed using a Cameca LEAP 3000X HR operating in laser-mode with a specimen temperature of 50 K and a pulse energy of 0.6–0.8 nJ.

2.2. Oxide dispersion strengthened steel–14YT

The oxide dispersion strengthened steel (referred to from here-on-in as 14YT) was prepared by the weighing and mixing of high purity of elemental powders (Fe, Ti, Cr and Y_2O_3) to give a composition of Fe–14Cr–0.2Ti–0.3Y $_2$ O $_3$ (all wt.%). The full composition is

given in Table 2. The solid solution hardener W was not included in this composition in order to study the fundamental radiation response of the nanoclusters with no contribution from the W. The mixed powders were mechanically alloyed by ball milling (Simolayer CM-08) in an argon atmosphere for 4 h at 1000 rpm with a ball-to-powder ratio of 10:1. The milled powder was consolidated by extrusion at 1150 °C and then quenched prior to being tempered at 750 °C for 2 h and air-cooled.

Following sample preparation and polishing the specimens were irradiated at the Indira Gandhi Centre for Atomic Research (IGCAR), Kalpakkam, India using 5 MeV Fe $^{3+}$ ions up to a total dose of 50 dpa at a temperature of 700 °C. The dpa was calculated based on SRIM calculations using the Kinchin–Pease model with a displacement energy E_d of 40 eV. Post ion-irradiation samples to be analysed by atom probe tomography were prepared from the bulk using a FIB technique [26]. The samples were then analysed using a Cameca 4000X HR in laser-mode with a specimen temperature of 50 K, pulse fraction of 20% and pulse energy of 0.3–0.4 nJ.

3. Results and discussion

3.1. Tungsten

Following ion irradiation of the W–3Re and W–5Re the data was analysed in a manner to search for evidence of clustering of the Re. A plot of the Re concentration distribution for the W–5Re un-implanted and 300 and 500 °C irradiated samples is shown in Fig. 1. The figure shows that for the conditions under which the specimen was irradiated (300 and 500 °C, 1.5 dpa), the distribution of the Re atoms is indistinguishable from that of the un-irradiated specimen i.e. the Re remains in solution and no segregation occurs (although improvements in detector efficiency should enable clusters containing 2–9 atoms to be identified [27]). This indicates that no clustering occurs in these samples and as such more focus will now be given to the W–25Re specimen.

Atom probe reconstructions of the W–25Re alloy following irradiation show strong evidence for cluster formation. These clusters are formed solely from the process of irradiation based on the lack of cluster formation following annealing of the un-irradiated alloys at 1200 °C for 12 h. Atom maps of the Re atoms from the W–25Re material irradiated to 1.5 dpa under 4 different conditions (300 °C, needle; 300 °C, bulk; 500 °C, needle; 500 °C, bulk) are shown in Fig. 2. Spatially separated clusters are evident throughout and it is particularly noticeable that the number density of the clusters is significantly higher in the lower, 300 °C, irradiation than in that of the 500 °C irradiation. In order to obtain more quantitative data on the clusters, the maximum separation method [28] was used to identify and separate the clusters from the matrix atoms. The

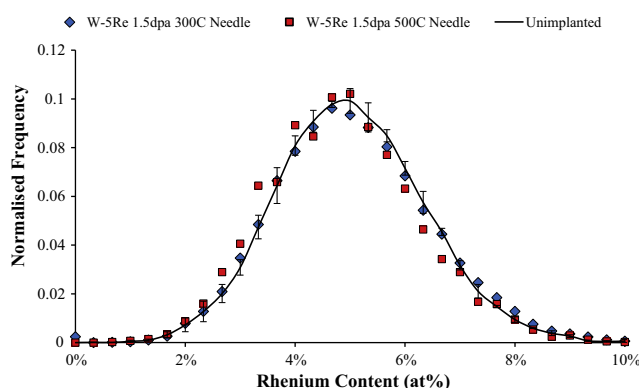


Fig. 1. Bulk rhenium concentration distribution in irradiated and non-irradiated W–5 wt.%Re.

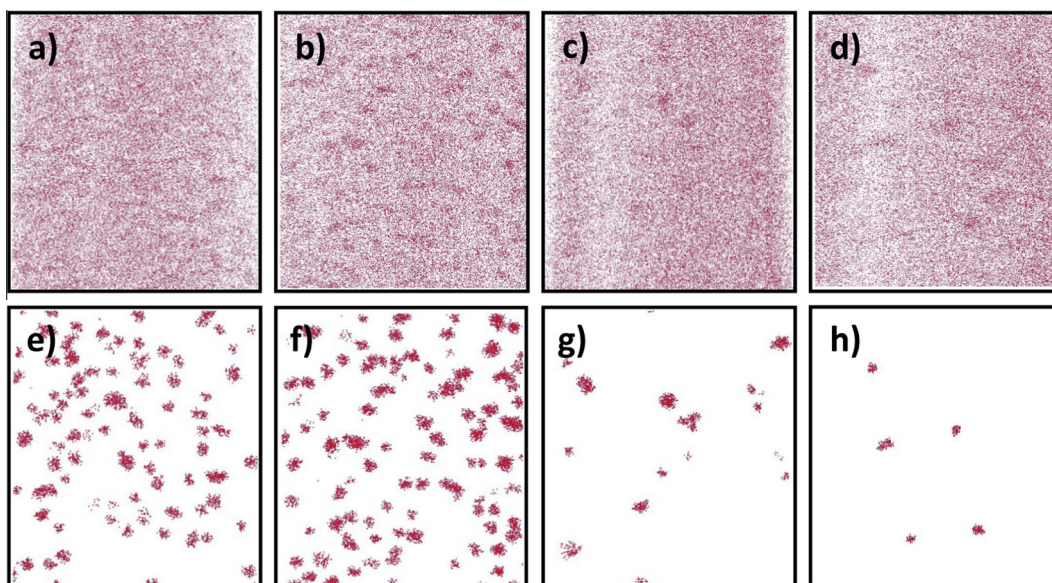


Fig. 2. Re atom map plots for (a and e) bulk, 300 °C; (b and f) needle, 300 °C; (c and g) bulk, 500 °C; and (d and h) needle, 500 °C, (a–d) shows all Re atoms detected within a rectangular volume ($40 \times 45 \times 6$ nm); bottom row shows only Re atoms contained within clusters.

values used for D_{max} (the maximum separation between solute atoms) and N_{min} (the minimum size of a cluster expressed in terms of solute atoms that constitutes a significant cluster) were 0.6 nm and 20 respectively. The results from this analysis (average cluster radius and number density), along with the averaged measured Re content from within the clusters is given in Table 1. What is clear from this table is that there is a difference in the average radii of the clusters arising from the different irradiation temperatures. There are variances in the average cluster size between the FIB-prepared and pre-sharpened needle specimens although no trend is discernable. Another notable observation is that there is also a significant difference in the number density of the clusters with a significantly reduced density for the 500 °C irradiated specimens. Again there is an observed variance in the number density between the FIB prepared and pre-sharpened needle specimens but no trend. However there is a trend in the Re content in the clusters with an increase in clustered Re in the higher temperature irradiations; and an increase in Re concentration between the bulk and needle irradiations.

Although the average cluster radius is a useful measure, the cluster size distributions are also extremely informative and the size distribution is given in Fig. 3. This plot shows that no clusters <1 nm diameter were detected, as were no clusters >4.2 nm. With the exception of the pre-sharpened needle irradiated to 1.5 dpa at 300 °C, the cluster sizes exhibit a skew-normal distribution. The pre-sharpened needle irradiated at 300 °C shows a Gaussian-type profile centred at a larger cluster diameter than the other irradiation conditions (2.5 nm compared to ~2 nm as per Fig. 3 and Table 1).

What is evident from these results is that for the irradiation conditions used, precipitates form only in the high Re content materials. This is in contrast to some previous work in which W

Table 1
Summary of the cluster composition, average diameter and number density for the irradiated W–25Re specimen.

	Re content (at.%)	Average diameter (nm)	Number density ($\times 1000/\mu\text{m}^3$)
1.5 dpa, 300 °C, bulk	32.6	2.04	7001
1.5 dpa, 300 °C, needle	34.5	2.34	7956
1.5 dpa, 500 °C, bulk	35.2	1.98	695
1.5 dpa, 500 °C, needle	43.6	1.85	264

Table 2

Composition of the oxide dispersion strengthened steel 14YT used in this study.

	Fe	Cr	Ti	Y	O	C	N	Si	Mn
at.%	87.3	11.5	0.25	0.19	0.69	0.02	0.07	0.01	0.03

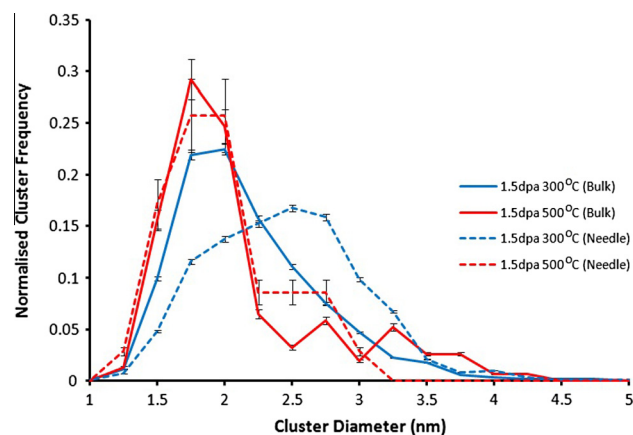


Fig. 3. Normalised plots of cluster size distribution for bulk and electropolished needle samples of W–25Re irradiated to 1.5 dpa at 300 and 500 °C.

alloys containing 3–5 at.% Re were also observed to form precipitates [9] when irradiated with neutrons at temperatures between 400 and 750 °C. The absence of precipitates in the present study indicates that at temperatures <400 °C, precipitation is inhibited in low Re content tungsten alloys.

Re is an under-sized atom when compared to W, and for this reason it will readily segregate to point defect sinks [9]. It is also possible for solutes to easily bond with matrix interstitials and form dumbbells. These solute–interstitial dumbbells can then drag the solute atom towards a point defect sink site [9]. Furthermore both Re and Os (transmutation products) have been shown to suppress void formation in irradiated tungsten [29]. Therefore it is possible that the irradiation-induced interstitials bond with the Re solute atoms within the matrix and migrate towards embryonic void sites (formed/forming due to the excess of vacancies remain-

ing in the matrix due to incomplete recombination of the interstitials and vacancies due to the interstitial–solute combination). The interstitial-Re dumbbells are then trapped by the void sites and begin to cluster together and form a precipitate.

Now looking at the average sizes of the precipitates formed, and the form of the material being irradiated (bulk or pre-sharpened needle), there is a difference in both the sizes and the compositions of the clusters. The proximity of free surfaces during irradiation is a well-known effect that has been well characterised during in-situ ion irradiation within transmission electron microscopes, and has been shown to enhance or retard radiation effects [30,31]. When irradiating a pre-sharpened needle of which the free surface is in close proximity to the volume from which the data sets are collected, similar perturbations of the radiation effects are expected to be seen. Due to the lack of trends, it is not possible within this study to determine the effects of the free surfaces on precipitate formation in W–Re alloys, but it does appear to be perturbing the composition and size data.

3.2. Oxide dispersion strengthened steel–14YT

Representative atom maps of the 14YT material from un-irradiated electropolished samples, un-irradiated FIB prepared samples and irradiated (50 dpa, 700 °C) samples are shown in Fig. 4. In these atom maps, only the Y, Ti and O are shown for clarity. Clusters comprising Y, Ti and O are observed in all cases as expected; some small levels are also observed in solid solution within the matrix. In all conditions the number density of the clusters are approximately the same with values in the $1 \times 10^{23} \text{ # m}^{-3}$ region, similar to other studies [18,20,32]. There appears to be very little, if any, variation in the morphology of the clusters. However there is a variation in size distribution of the clusters, as shown in Fig. 5. It can be seen that both un-irradiated samples have similar characteristics: a main peak around 1.3–1.5 nm radius, minimum radii of ~ 0.5 nm and a maximum radii of ~ 5 nm (some larger clusters are observed in the electropolished samples, but this could be due to the relatively small sampling volumes not having larger clusters within those volumes). The irradiated sample shows a different size distribution with a significant number of clusters having a radii of ~ 1.75 nm, minimum radii of ~ 0.5 nm and a maximum radii of 4.5 nm. This suggests that the irradiation is having an effect on the size of the clusters. To investigate this further it is desirable to have information on the compositions of the clusters. Previous work has shown that the primary elements within clusters in oxide dispersion strengthened steels of similar compositions are Y, Ti and

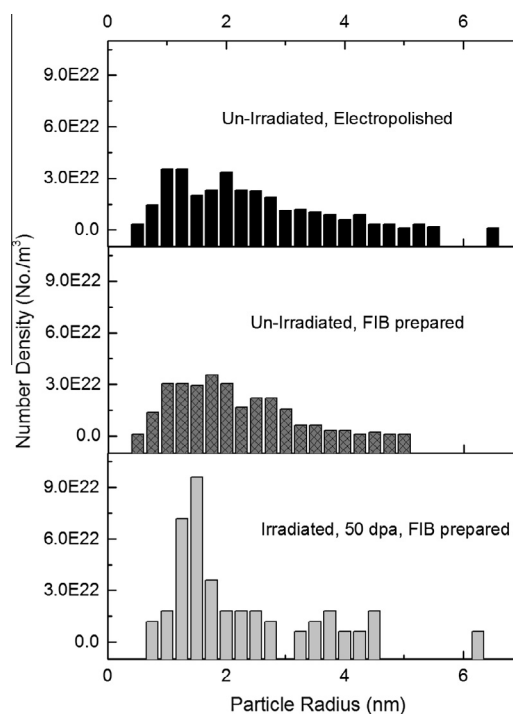


Fig. 5. Histogram plots of the number density of particles with specific radii for the three different conditions: un-irradiated and electropolished, un-irradiated and FIB prepared, and irradiated to 50 dpa and FIB prepared.

O [33]. The normalised relative composition of the Y, Ti and O averaged over the entire data set for each condition examined is given in Table 3. In the un-irradiated cases there is no discernable difference in the relative compositions of the clusters, however following irradiation compositional changes have occurred. The O content remains similar to the as irradiated case, but the Y has reduced and the Ti increased. A plot of the relative cluster appearance in the data sets as a function of the Y:Ti ratio is given in Fig. 6. From this graph it can be seen that there is a shift of the most common Y:Ti ratios to lower Y:Ti ratios in the order of: un-irradiated FIB prepared, un-irradiated electropolished, and irradiated and FIB prepared.

Examining the data presented in Figs. 5 and 6 focussing on the un-irradiated results, there is a change in the composition of the material whilst no significant change in cluster size distribution is seen. This can mean two possibilities: firstly the cluster composition of the two specimens is slightly dissimilar, which may be possible given the inhomogeneous distributions seen in similar materials [19,34]; and secondly that irradiation-induced damage created by the FIB process has altered the cluster composition. FIB induced radiation damage can be ruled out as affecting the composition in this case as the data for the heavy ion irradiation to 50 dpa shown in the same figure shows that the Y:Ti ratio is reduced rather than increased as seen in the FIB prepared specimens suggesting that this is not the mechanism by which the composition is altered, hence it is most likely that the variance in composition is due to manufacturing processes. What is evident is the significant change in Y:Ti ratio following irradiation to 50 dpa (also evident in the average cluster compositions given in Table 3) and the change in the cluster sizes. The stability of nano-scale oxide particles in steels under irradiation has been examined extensively in recent times, e.g. [16,19,21,22,32,34–37], focussing on their structure and composition. Whilst the structure/composition of the oxide particles has not yet been definitively identified, the pyrochlore structures $\text{Y}_2\text{Ti}_2\text{O}_7$ (2–2–7) and Y_2TiO_5 (2–1–5) have been suggested to be the most predominant forms. The

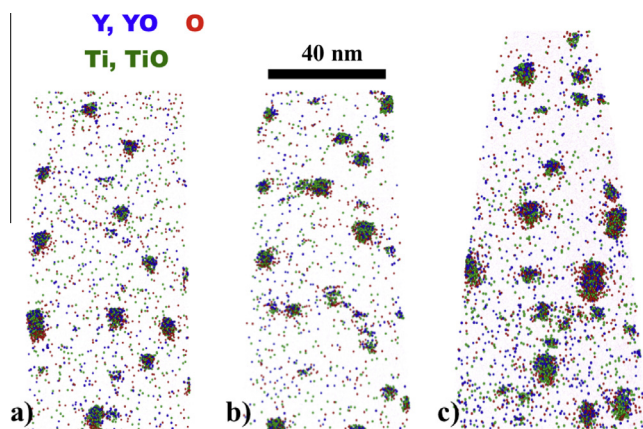
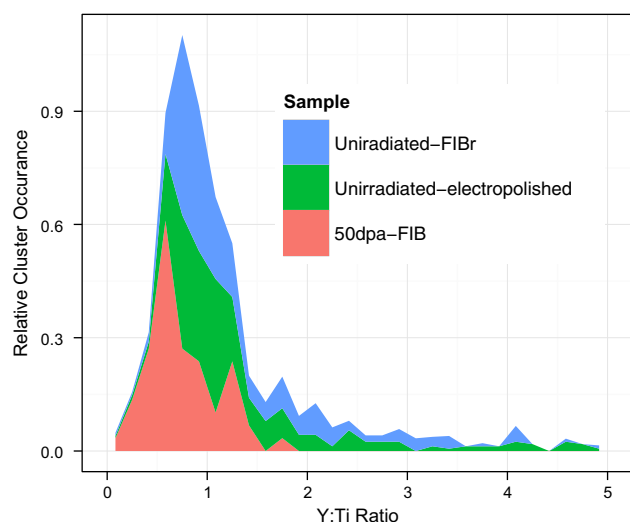


Fig. 4. Atom maps of the ODS–14YT material showing only Y, Ti and O atoms. Data was collected from (a) un-irradiated electropolished needle, (b) un-irradiated FIB prepared needle, and (c) irradiated (50 dpa, 700 °C) FIB prepared needle.

Table 3

Cluster number density and average cluster relative composition of Y, Ti and O as determined from the atom probe data. The number given in the parentheses is the standard deviation.

	Cluster number density ($1 \times 10^{23} \text{ \#}/\text{m}^{-3}$)	Y	Ti	O
Un-irradiated, electropolished	3.0	0.24 (0.10)	0.19 (0.06)	0.57 (0.06)
Un-irradiated, FIB prepared	2.7	0.23 (0.09)	0.17 (0.06)	0.59 (0.05)
Irradiated to 50 dpa, FIB prepared	3.7	0.18 (0.06)	0.27 (0.07)	0.55 (0.06)

**Fig. 6.** Plot of the relative cluster sizes for various Y:Ti ratios.

un-irradiated Y:Ti ratios as given in Table 3 agree somewhat with the 2-2-7 and 2-1-5 compositions (within the measurement errors), whereas the irradiated compositions varies between the stoichiometric 2-2-7 and sub-stoichiometric i.e. Y:Ti < 1, values. This possibly indicates that the smaller clusters that are more dominant in the irradiated material are sub-stoichiometric pyrochlore.

The reduced Y:Ti ratio also suggests that the clusters are becoming enriched with Ti/deplete of Y during the irradiation. This is most likely due to the ballistic collision process of the ion irradiation driving the elements of the cluster into the matrix. At high temperature the cluster elements can back-diffuse and re-form the cluster whilst at lower temperatures this back-diffusion is inhibited [20]. During the irradiations performed in this study (at 750 °C) it is possible that ballistic mixing occurs and that the diffusion of Y is retarded over the temperature/time period of the experiment resulting in incomplete reformation of the cluster. This reduction in Y:Ti possibly suggests that Ti_2YO_5 forms as a result of the irradiation.

4. Conclusion/summary

Cluster formation in two materials for use in advanced nuclear reactor systems – a tungsten–rhenium alloy and an oxide dispersion strengthened steel – has been investigated by atom probe tomography. For the tungsten–rhenium alloy irradiation induced clustering is not observed in the low Re content materials, but is for the Re 25 at.% alloy. When comparing irradiations carried out on pre-sharpened needles and bulk specimens a variance in the cluster sizes and number density was observed, but it was not possible to deduce any trends. For the steel specimens, the oxide particles sizes and composition were comparable when prepared through conventional electropolishing and FIB techniques. Following irradiation, the oxide particles were observed to refine to smaller sizes and the Y:Ti ratio reduced. It is suggested that a Ti_2YO_5 particle may be prevalent after irradiation.

Acknowledgements

The authors would like to acknowledge support from the UK's Engineering and Physical Sciences Research Council (EPSRC) for funding under Grant Reference EP/H018921/1. PDE acknowledges support through an EPSRC Career Acceleration fellowship (EP/K030043/1).

References

- [1] S.J. Zinkle, G.S. Was, *Acta Mater.* 61 (2013) 735–758.
- [2] S.J. Zinkle, J.T. Busby, *Mater. Today* 12 (2009) 12–19.
- [3] D.E.J. Armstrong, P.D. Edmondson, S.G. Roberts, *Appl. Phys. Lett.* 102 (2013) 251901–251925.
- [4] M.R. Gilbert, S.L. Dudarev, S. Zheng, L.W. Packer, J.-C. Sublet, *Nucl. Fusion* 52 (2012) 083019.
- [5] J.W. Davis, V.R. Barabash, A. Makhankov, L. Plöchl, K.T. Slattery, *J. Nucl. Mater., Part 1* 258–263 (1998) 308–312.
- [6] M.R. Gilbert, J.-C. Sublet, *Nucl. Fusion* 51 (2011) 043005.
- [7] A. Giannattasio, S.G. Roberts, *Philos. Mag.* 87 (2007) 2589–2598.
- [8] A. Giannattasio, Z. Yao, E. Tarleton, S.G. Roberts, *Philos. Mag.* 90 (2010) 3947–3959.
- [9] T. Tanno, A. Hasegawa, M. Fujiwara, J.-C. He, S. Nogami, M. Satou, T. Shishido, K. Abe, *Mater. Trans.* 49 (2008) 2259–2264.
- [10] G.R. Odette, M.J. Alinger, B.D. Wirth, *Annu. Rev. Mater. Res.* 38 (2008) 471–503.
- [11] G.R. Odette, D.T. Hoelzer, *Mater. Nucl. Power* 62 (2010) 84–92.
- [12] P.D. Edmondson, C.M. Parish, Q. Li, M.K. Miller, *J. Nucl. Mater.* 445 (2014) 84–90.
- [13] P.D. Edmondson, C.M. Parish, Y. Zhang, A. Hallén, M.K. Miller, *Scr. Mater.* 65 (2011) 731–734.
- [14] P.D. Edmondson, C.M. Parish, Y. Zhang, A. Hallén, M.K. Miller, *J. Nucl. Mater.* 434 (2013) 210–216.
- [15] G.R. Odette, P. Miao, D.J. Edwards, T. Yamamoto, R.J. Kurtz, H. Tanigawa, *J. Nucl. Mater.* 417 (2011) 1001–1004.
- [16] M. Miller, C. Fu, M. Krcmar, D. Hoelzer, C. Liu, *Front. Mater. Sci. China* 3 (2009) 9–14.
- [17] M.K. Miller, C.M. Parish, Q. Li, *Mater. Sci. Technol.* 29 (2013) 1174–1178.
- [18] M. Miller, C.M. Parish, *Mater. Sci. Technol.* (2011) 729–734.
- [19] A. Certain, S. Kuchibhatla, V. Shutthanandan, D.T. Hoelzer, T.R. Allen, *J. Nucl. Mater.* 434 (2013) 311–321.
- [20] C.M. Parish, P.D. Edmondson, Y. Zhang, M.K. Miller, *J. Nucl. Mater.* 418 (2011) 106–109.
- [21] M.K. Miller, D. Hoelzer, K.F. Russell, *Mater. Res. Soc. Symp. Proc.* 1215 (2009) 1215-V1206–1202.
- [22] M.K. Miller, Y. Zhang, *Ultramicroscopy* 111 (2011) 672–675.
- [23] C.B. Beck, S.G. Roberts, P.D. Edmondson, D.E.J. Armstrong, *Mater. Res. Soc. Symp. Proc.* 1514 (2013) 99–104.
- [24] J.F. Ziegler, *J. Appl. Phys.* 85 (1999) 1249–1272.
- [25] ASTM, Standard Practice for Neutron Radiation Damage Simulation by Charged-Particle Irradiation, in E521-96(2009), vol. e1, 2009, West Conshohocken, PA.
- [26] M.K. Miller, K.F. Russell, *Ultramicroscopy* 107 (2007) 761–766.
- [27] M.K. Miller, D. Reinhard, D.J. Larson, *J. Nucl. Mater.* (this special issue).
- [28] J.M. Hyde, E.A. Marquis, K.B. Wilford, T.J. Williams, *Ultramicroscopy* 111 (2011) 440–447.
- [29] V.K. Sikka, J. Moteff, *J. Appl. Phys.* 42 (1972) 4942–4944.
- [30] P.D. Edmondson, D.J. Riley, R.C. Birtcher, S.E. Donnelly, *J. Appl. Phys.* 106 (2009) 043505–043508.
- [31] J.S. Williams, M.J. Conway, J. Wong-Leung, P.N.K. Deenapanray, M. Petravic, R.A. Brown, D.J. Eaglesham, D.C. Jacobson, *Appl. Phys. Lett.* 75 (1999) 2424–2426.
- [32] C.M. Parish, L. Yao, Y. Zhang, P.D. Edmondson, A. Hallén, M.K. Miller, *Microsc. Microanal.* 18 (Suppl. 2) (2012) 1430–1431.
- [33] M.K. Miller, E.A. Kenik, K.F. Russell, L. Heatherly, D.T. Hoelzer, P.J. Maziasz, *Mater. Sci. Eng., A* 353 (2003) 140–145.
- [34] A.G. Certain, K.G. Field, T.R. Allen, M.K. Miller, J. Bentley, J.T. Busby, *J. Nucl. Mater.* 407 (2010) 2–9.
- [35] R.L. Klueh, J.P. Shingledecker, R.W. Swindeman, D.T. Hoelzer, *J. Nucl. Mater.* 341 (2005) 103–114.
- [36] M. Kolluri, P.D. Edmondson, N.V. Luzginova, F.A.v.d. Berg, *Mater. Sci. Eng., A* 597 (2014) 111–116.
- [37] M. Kolluri, P.D. Edmondson, N.V. Luzginova, F.A.v.d. Berg, *Mater. Sci. Technol.* 30 (2014) 1697–1703.